Sonoluminescence and acoustic cavitation

メタデータ	言語: eng 出版者: 応用物理学会 公開日: 2019-03-27 キーワード (Ja): キーワード (En): 作成者: 崔, 博坤 メールアドレス: 所属:
URL	http://hdl.handle.net/10291/20037

This review paper was published in
Japanese Journal of Applied Physics, vol.56, 07JA01(9 pages), 2017
(https://doi.org/10.7567/JJAP.56.07JA01)
Copyright 2017 The Japan Society of Applied Physics

Sonoluminescence and acoustic cavitation

Pak-Kon Choi*
Department of Physics, Meiji University
1-1-1 Higashimita, Tama-ku, Kawasaki, 214-8571, Japan

Abstract

Sonoluminescence (SL) is light emission under high-temperature and high-pressure conditions of a cavitating bubble under intense ultrasound in liquid. In this review, the fundamentals of the interactions between the sound field and the bubble, and between bubbles are explained. Experimental results on high-speed shadowgraphy of bubble dynamics and multibubble SL are shown, demonstrating that the SL intensity is closely related to the bubble dynamics. SL studies of alkali-metal atom (Na and K) emission are summarized. The spectral measurements in solutions with different noble-gas dissolutions and in surfactant solutions, and the results of spatiotemporal separation of SL distribution strongly suggested that the site of alkali-metal atom emission is the gas phase inside bubbles. The spectral studies indicated that alkali-metal atom lines are composed of two kinds of lines: a component that is broadened and shifted from the original D lines arises from van der Waals molecules formed between alkali-metal atoms and noble-gas atoms under extreme conditions at bubble collapse. The other spectral component exhibiting no broadening and no shift was suggested to originate from higher temperature bubbles than those producing the broadened component.

Key words: sonoluminescence, acoustic cavitation, bubble dynamics, alkali-metal atom emission, Bjerknes force, high-speed shadowgraphy

*E-mail: pkchoi@meiji.ac.jp

1. Introduction

The irradiation of liquid with a high-intensity ultrasound causes acoustic cavitation, i.e., the formation and oscillation of bubbles. The expansion and contraction of bubbles occur in phase with the sound pressure, generating high-temperature and high-pressure conditions at bubble collapse in the process of adiabatic compression[1-4]. The violent bubble oscillation induces the formation of hydroxyl (OH) radicals and sometimes an emission of luminescence (sonoluminescence, abbreviated as SL). Frenkel and Schultes[5] discovered that a faint luminescence accompanied the fogging of a photographic plate immersed in a water bath, which was subjected to a high-intensity ultrasound. The term "sonoluminescence" was named by Harvey[6], who explained that the luminescence was caused by electrical discharge at the collapse of charged bubbles. Several theories have been proposed for the mechanism explaining the SL emission, including the electrical microdischarge theory, the mechanochemical theory, the triboluminescent theory, the chemiluminescent theory, the hot spot theory, and the shock wave theory[1]. At present, the hot spot theory is widely accepted. Owing to the quasi-adiabatic process of bubble oscillation, high-temperature and high-pressure conditions inside the bubble are achieved. These conditions produce ionization of noble-gas molecules, resulting in bremsstrahlung (break radiation in English)[2].

The dynamics of acoustic cavitation bubbles has been extensively investigated[7,8]. Equations governing the spherical oscillation of a single bubble include the famous Rayleigh-Plesset equation. Acoustic field–bubble and bubble–bubble interactions are described by the primary and secondary Bjerknes forces[9], respectively, causing bubbles to self-organize into various structures, such as filaments, jellyfishes, streamers, clusters, and clouds. The occurrence of multibubble sonoluminescence (MBSL) is greatly affected by the bubble dynamics, which depends on acoustic frequency and acoustic pressure. The spatial distribution of MBSL is determined by acoustic-field distribution.

The application of acoustic cavitation to chemistry has been studied since the famous work by Wood and Loomis[10] in 1927. The chemical effect by acoustic cavitation is called sonochemistry[11,12], which deals with phenomena and reactions induced by radicals formed in and around bubbles from the thermal decomposition of molecules and by shock waves generated by rapidly released localized pressure. The extraordinary high temperature and pressures together with the heating and cooling rates above 10^{10} K/s at bubble collapse provide a high-energy reaction field. Nowadays, the area of sonochemistry extends to biological[13-16], medical[17-19], environmental[20-29], food technologies[30], and others.

This review presents the fundamentals of bubble dynamics and recent studies on MBSL in relation to bubble dynamics. Furthermore, MBSL studies of alkali-metal atom lines are extensively described. Alkali-metal atom ions (Na+ or K+, for example) in solution are nonvolatile and hence do not enter bubbles directly. The site of alkali-metal atom lines has been an issue in question for a long time.

2. Acoustic bubble and bubble dynamics

The expansion and contraction of bubble under ultrasound irradiation can be formulated using the

Rayleigh-Plesset equation[1]. On the basis of this equation, Keller and Miksis[31] derived a similar equation for large-amplitude forced radial oscillations of a bubble as follows.

$$\left(1-\frac{1}{c}\dot{R}\right)R\ddot{R}+\frac{3}{2}\left(1-\frac{1}{3c}\dot{R}\right)\dot{R}^2$$
$$=\frac{1}{\rho}\left(1+\frac{1}{c}\dot{R}+\frac{R}{c}\frac{d}{dt}\right)\times\left\{\left(P_{g0}+\frac{2\sigma}{R_0}\right)\left(\frac{R_0}{R}\right)^{3\gamma}-P_0-\frac{2\sigma}{R}-\frac{4\mu\dot{R}}{R}-P(t)\right\} \quad (1)$$

Here, R is the instantaneous bubble radius and R0 is the ambient radius. P_0 and P(t) are the static and sound pressures in liquid, respectively. σ is the surface tension, c is the sound velocity, ρ is the density, and μ is the viscosity of the liquid. P_{g0} is the initial value of gas pressure in the bubble, and γ is the polytropic index. The value of γ takes an intermediate value between the ratio of the specific heat of the gas and unity, depending on whether the gas is behaving adiabatically, isothermally, or in some intermediate manner. Using Eq. (1), we have calculated bubble radii in water for an acoustic frequency of 24 kHz and acoustic pressures of 0.8, 1, 1.2, and 1.4 atm, R0=5 μm, and γ=5/3 assuming an adiabatic change of noble gas. Figure 1 shows the calculated results of the time dependences of acoustic pressure (upper trace) and bubble radius (lower traces). Here, T is the sound period, which equals 42 μs in this calculation. The maximum radius for the case of 1.4 atm is approximately 50 μm and the minimum radius is less than 0.6 μm. Kozuka et al.[32] demonstrated using the direct stroboscopic observation of a sonoluminescing bubble that the experimental values of bubble diameter fitted well with the Keller-Miksis equation. On the basis of the adiabatic change of state, the maximum temperature and pressure are achieved at a minimum bubble radius Rmin, and can be predicted by

$$T_{max}=T_0\left(\frac{R_0}{R_{min}}\right)^{3(\gamma-1)} \quad (2)$$

$$P_{max}=P_{g0}\left(\frac{R_0}{R_{min}}\right)^{3\gamma} . \quad (3)$$

Here, T_0 and P_{g0} are the temperature and pressure, respectively, of gas in the bubble in the absence of a sound field. The calculations utilizing Eqs. (2) and (3) with typical parameters give Tmax≈ 20,000 K and P_max≈1000 atm. These values may be overestimated, since the perfect adiabatic process

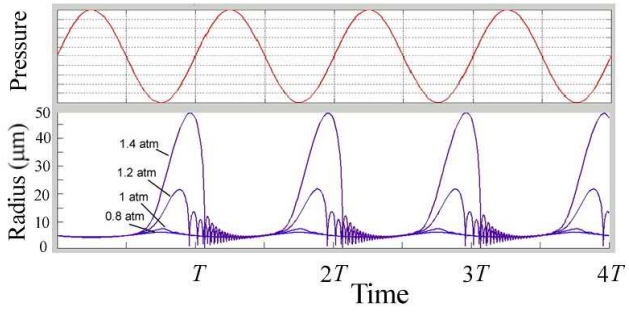

Fig. 1. Acoustic pressure (upper) and bubble radius (lower) vs. time curves calculated using eq. (1) for four acoustic cycles. The acoustic frequency is 24 kHz and pressure is varied from 0.8 to 1.4 atm. Initial bubble radius is 5 μm.

would not be realized. Furthermore, water vapor and gases inside bubbles lower the maximum temperature. The thermal decomposition of water molecules generates hydroxyl and hydrogen radicals and these reactions consume energy, resulting in a decrease in the temperature. For example, adding a small quantity of alcohol molecules decreases the SL intensity, because the bubble final temperature decreases owing to the thermal decomposition of alcohol molecules that evaporated into bubbles[33]. However, Eqs. (2) and (3) give a rough indication of where the maximum temperature and pressure are located.

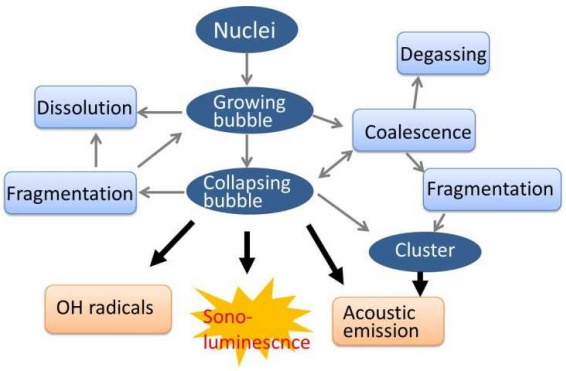

Fig. 2. Schematic illustration of "Life of bubbles". Reprinted with permission from ref. (10). Copyright 2016 by Springer.

The generation of bubbles by acoustic cavitation is elucidated as follows. Bubble nuclei adhered to dust in a liquid, or to a container wall, grow into small bubbles by the rectified diffusion of gas dissolved in the liquid under acoustic pressure. These bubbles are denoted as "growing bubbles" in Fig. 2, which schematically shows the"life of bubbles". Some growing bubbles may dissolve in the liquid because of surface tension, and other bubbles may further grow into "collapsing bubbles," which oscillate violently. Note that "collapsing" does not necessarily mean bubble extinction. The collapsing bubble may cause nonspherical oscillation because of its strong nonlinearity. This leads to fragmentation into small bubbles. The collapsing bubbles may cause each other to coalesce via the secondary Bjerknes force, and sometimes form a bubble cluster or a bubble cloud. The conditions inside the collapsing bubble are high temperature and high pressure, which may produce OH radicals through the decomposition of water molecules. OH radicals transfer through the liquid/bubble interface and interact with foreign molecules surrounding the bubble. The oxidation reaction of luminol molecules by OH radicals produces blue light emission, known as sonochemiluminescence. When the conditions at bubble collapse are extreme, light emission due to bremsstrahlung of electrons occurs. Oscillations of the bubble wall produce pressure waves and sometimes shock waves propagating in a liquid (acoustic emission). Most of the kinetic energy of the bubble oscillations is transformed into the energy of acoustic emission. The oscillation energy of a bubble is spatiotemporally concentrated in a very small region less than 1 μm^3 and to the time duration of ~100 ps. The energy concentration through the bubble oscillation may be the key process of SL and sonochemistry.

Sound field-bubble interaction is called primary Bjerknes force. The force acting on a bubble under

acoustic field is given by[9)]

$$F_{B1} = -\langle V(t)\nabla p\rangle, \qquad (4)$$

where V(t) is the time-dependent bubble volume, ∇p is the gradient of acoustic pressure and ‹› stands for the time averaging operation during an acoustic cycle. In a standing wave field, the bubble moves towards antinode of the acoustic field if the bubble is smaller than the resonant size[34)]. Figure 3 illustrates a photograph of SL emitted from those bubbles positioned in antinodes established in a cylindrical container. Sample liquid is water dissolved with argon gas. An acoustic frequency is 151 kHz.

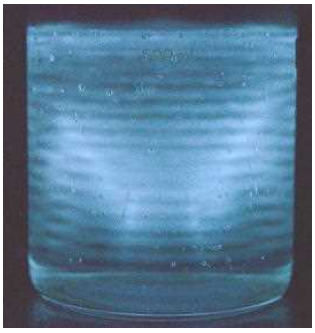

Fig. 3 (Color online) Sonoluminescence from argon-saturated water at a frequency of 151 kHz in a cylindrical container. Luminescence is emitted from the bubbles trapped at antinodes of a standing-wave field.

Oscillating bubble 1 emits sound, which acts on another bubble 2. This bubble-bubble interaction is called the secondary Bjerknes force:

$$F_{B2} = -\langle V_2\nabla p_1\rangle = -\frac{\rho}{4\pi r^2}\langle \dot{V}_1\ \dot{V}_2\ \rangle, \qquad (5)$$

where V_2 is the volume of bubble 2, and p_1 is the acoustic pressure from bubble 1. $\dot{V}_1$ and $\dot{V}_2$ are the volume change rates of two bubbles, r is the distance between the two bubbles, and ρ is the density of the liquid. According to eq. (5), a bubble smaller than the resonance radius and a bubble larger than the resonance radius repel each other, while pairs of bubbles smaller or larger than the resonance radius attract each other. A high-speed shadowgraph observation of the two-bubble interaction is shown in Fig. 4. The frame rate of a high-speed camera was 1 M fps. Two bubbles attract each other while oscillating in phase under 87 kHz ultrasound field. The relative distance r and approaching velocity were analyzed from the frames in Fig.4, and are shown in Fig. 5 together with the time dependences of bubble diameter. The approaching velocity increases at the instances of the decrease in two bubble volumes, and increases with decreasing the relative distance. The experimental observation of two bubble interaction is well explained by the prediction using eq. (5).

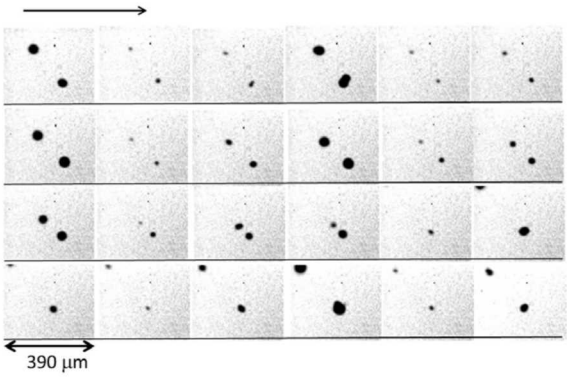

Fig. 4. Two acoustic bubbles exhibiting attraction and coalescence under 87 kHz ultrasound at acoustic power of 5 W in water. The frames were selected from the video captured at 1 M fps so that the frame

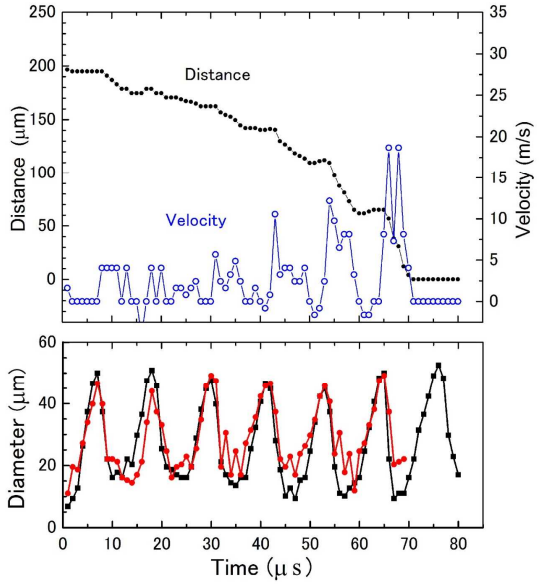

Fig. 5. The relative distance r and approaching velocity of two bubbles shown in Fig. 4. The lower curves show the time dependences of the bubble diameter. The phase difference of bubble oscillations in the range of 10–20 μs was caused by asymmetrical oscillation.

3. Dependence of sonoluminescence on bubble dynamics

The intensity of multibubble SL depends on bubble dynamics, which is dependent on acoustic frequency, pressure amplitude, and acoustic-field geometry. Henglein and Gutierrez[35] demonstrated that the yield of iodine during KI oxidation due to OH radicals showed a maximum when measured as a function of acoustic power. Hatanaka et al.[36] observed that the MBSL intensity decreases at high powers at 132 kHz. Tran et al.37) reported that liquid height is an important factor causing mechanical and chemical effects at 20 kHz. Uemura et al.[38] showed that an acoustic streaming also influences the SL intensity.

Lee and Choi[39] investigated the power dependences of SL intensity in relation to the corresponding bubble dynamics. They observed SL intensity in water at a frequency of 84 kHz by integrating the whole SL image pixels captured by a digital camera. The power dependence of the SL intensity showed a maximum and then decreased to zero as shown in Fig. 6. The reduction in SL intensity was confirmed in the three cases of a free liquid surface, a liquid surface covered with PET film, and a stainless steel plate surface, indicating that surface deformation due to acoustic radiation

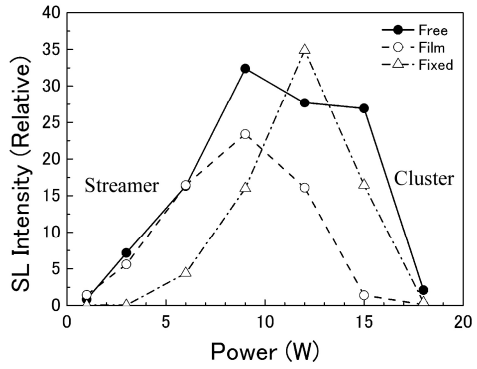

Fig. 6. Power dependences of SL intensity for boundary conditions of a free liquid surface (closed circles), a liquid surface covered with PET film (open circles), and stainless steel-plate surface (triangles). Reprinted with permission from ref. (35). Copyright 2014 by Elsevier Publishing.

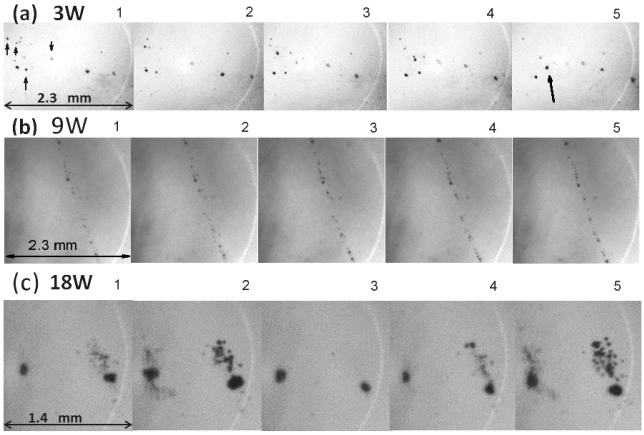

Fig. 7. Selected images from high-speed photography videos taken at a speed of 64 k fps. (a) Bubble streamer observed at a power of 3 W. Five frames with an interval of 190 μs were selected to illustrate bubble coalescence. The bubbles denoted by arrows in frame 1 coalesce into single bubble in frame 5. (b) Streaming bubbles observed at a power of 9 W. The frame interval is 48 μs. (c) Bubble clusters observed at a power of 18 W. The frame interval is 16 μs. Reprinted with permission from ref. (35). Copyright 2014 by Elsevier Publishing.

is not the cause of the SL reduction. The power dependence of the SL intensity was strongly correlated with the bubble dynamics captured by high-speed photography at 64 k fps. In the low-power range where the SL intensity increases, bubble streamers dominate and the population of streaming bubbles increased with power. At powers after the SL maximum occurred, bubble clusters came into existence. Upon complete SL reduction, only bubble clusters were observed. Selected bubble images shown in Fig. 7 demonstrate this correlation. In Fig. 7(a) captured at 3 W, only streaming bubbles were observed while repeating coalescence and fragmentation. In Fig. 7(b) captured at 9 W, the population of streaming bubbles increased. In Fig. 7(c) captured at 18 W, no streaming bubbles but only clusters were observed. The cluster was composed of tiny bubbles and a large bubble. The tiny bubbles exhibited an inertial (transient) cavitation in which the bubble collapsed violently and disintegrated into small bubbles. Some may be large enough to renucleate and repeat the inertial cavitation. Some

oscillation cycles are needed to emit SL. The large bubble oscillates nonspherically and does not collapse violently. The cluster emits large subharmonic and broadband spectra of acoustic emission.

4. Mechanism of sonoluminescence

4.1 Single bubble sonoluminescence

An adiabatic compression of bubble causes a high temperature condition of approximately 10,000 K at bubble collapse[2,3]. This is called the hot spot model. The temperature inside bubble is almost homogeneous across the bubble radius. The high temperature produces hot plasma (electrons and ions) by the ionization of argon atom, which is contained in air by an amount of 0.9%. A bremsstrahlung caused by the slowing down of electron speed is the origin of single-bubble SL (SBSL). The spectrum of SBSL is continuous and very broad extending from ultraviolet to near infrared wavelengths. Alternatively, shock waves may be generated if the bubble wall velocity exceeds sound velocity in a gas inside the bubble. This is a possible mechanism for establishing the high temperature condition. The temperature attained by this shock wave model can be 10^5–10^6 K. In the studies of SBSL in sulfuric acid, Suslick and coworkers[40,41] reported that the atomic emission of noble gas was observed, suggesting that a hot optically opaque plasma is formed in the bubble core, the temperature of which is not explained by the hot spot model.

Molecular emission from electronically excited state of hydroxyl (OH) radical can be observed in SBSL. Young et al. [42] found the weak OH line at 310 nm from water at very low acoustic pressure. Xu and Suslick [43] estimated the temperature of OH emission by the comparison of experimental spectra obtained in phosphoric acid with synthetic rovibronic spectra of $A^2\sum^+$–$X^2\Pi$ transition. Figure 8 shows the result of OH spectra from 65% phosphoric acid dissolved with various noble gases. The estimated temperatures were 6000, 7200, 8300 and 9600 K for He, Ne, Ar and Kr dissolution, respectively. The temperature increases with increasing atomic mass of noble gas, which corresponds to the decreasing order of the thermal conductivity. When a bubble undergoes compressional heating, the extent of adiabaticity will depend on the thermal conductivity of the gas in the bubble. Thus, the thermal conductivity affects the thermal transport from the heated gas to the cold surrounding liquid. A noble gas with small thermal conductivity will increase the SL intensity..

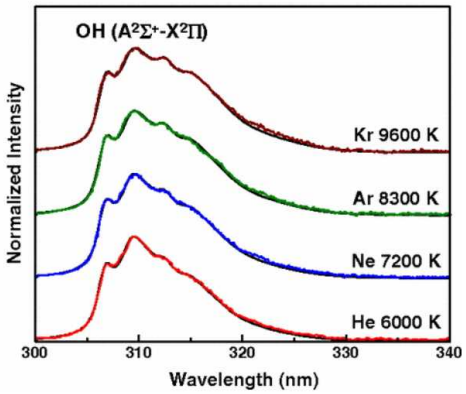

Fig. 8. (Color online) OH rovibronic spectra from 65% phosphoric acid dissolved with different noble gases at acoustic pressure of 2.4 bar. The OH emission temperature was higher for the smaller value of thermal conductivity of noble gas.
Reprinted with permission from ref. (43). Copyright 2010 by American Physical Society

4.2 Multibubble sonoluminescence

In a multibubble field, not only the primary Bjerknes force but also the secondary Berknes force is important to understand the bubble dynamics, as described in Sec. 2. A bubble size distribution exists as a result of bubble coalescence and fragmentation. Figure 9 shows MBSL spectra from argon-saturated water and NaCl aqueous solution with the concentration of 2 M. The ultrasonic frequency was 134 kHz and the applied acoustic power was 8.9 W. The MBSL spectrum from water exhibits both the continuous component and OH line, suggesting that there are different kinds of bubble population: the bubbles of higher emission temperature and those of lower emission temperature. In the NaCl solution, alkali-metal atom (Na in this case) emission is eminent in addition to the continuum. Abe and Choi44) demonstrated that the bubbles radiating Na emission are different from those radiating the continuous component. Figure 10(a) shows an SL photograph from 2 M NaCl aqueous solution in a cylindrical container at a frequency of 137 kHz. Using the process of RGB split, the spatial distribution of Na emission was obtained as a red component (b). Similarly, the spatial distribution of the continuous component was obtained as a blue component (c). Images (b) and (c) clearly suggest the different bubble populations of Na and the continuum emissions. They also showed that the time separation of SL pulses of Na and the continuum emission indicated that the bubbles radiating Na emission are larger in size and lower in temperature at collapse compared with those radiating the continuum emission.

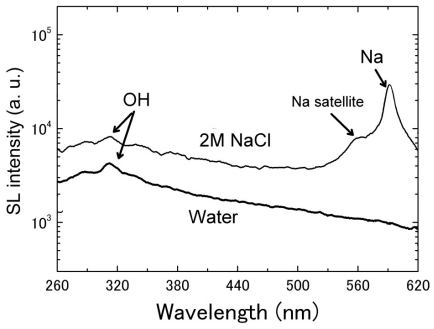

Fig.9. MBSL spectra from water and 2M NaCl aqueous solution at an acoustic frequency of 138 kHz and a power of 8.9 W.

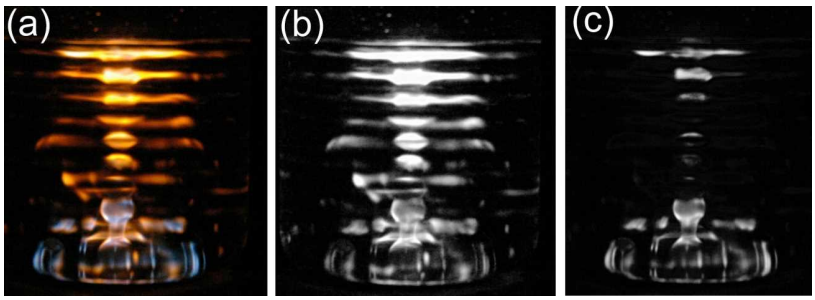

Fig.10. (Color online) (a): Sonoluminescence from 2 M NaCl aqueous solution in a cylindrical container at a frequency of 137 kHz. (b): Red component after RGB split of image (a) indicating the spatial distribution of Na emission. (c): Blue component after RGB split of image (a) indicating the spatial distribution of the continuous component. ref. (44). Copyright 2009 by the Japan Society of Applied Physics.

4.3 Mutibubble sonoluminescence from alkali-metal salt solution

It is important to clarify the mechanism for the SL of nonvolatile metal ions, which will be very useful for understanding the sonochemistry of nonvolatile species in aqueous solution. SL from an aqueous solution of alkali-metal salt such as NaCl or KCl has long been a topic of interest[45] since Günther et al.[46] found Na D lines in their MBSL study in 1957. To observe Na emission of D lines at 589.0 and 589.6 nm, Na+ ions dissolved in water must be reduced at some location. The site of Na emission has been discussed. There are two possibilities of the origin: the gas phase inside bubbles or the hot liquid phase at the liquid/bubble interface. Unlike alcohol or water molecules, nonvolatile species such as Na+ ions hardly enter the bubble interior by evaporation. On the basis of the gas phase origin, Sehgal et al.[47] reported the first experimental estimates of cavity temperature and pressure from the line broadening and shift of Na and K atom emissions in argon-saturated alkali-metal salt solutions sonicated at 460 kHz. The resonance line of emitting species undergoes pressure-induced broadening and shift due to the perturbation of its energy levels by neighboring atoms. Sehgal et al. obtained a relative density of 36, from which the emission temperature of 3400 K and the pressure of 310 atm were deduced.

Flint and Suslick [48] investigated the effects of solvent vapor pressure and dissolved-gas thermal conductivity on the line width and shift of K emission in primary alcohols and in water. The effect of a dissolved gas or impurity on alkali-metal atom emission provides important information about the site of the emission. The line width and peak position were independent of the change of the dissolved gas, although the cavitation condition was affected by the change of the dissolved gas. Flint and Suslick proposed that alkali-metal atom emission arises from rapidly heated fluid immediately surrounding the collapsing bubble.

Conversely, Lepoint-Mullie et al.[49] suggested the gas-phase origin from the results on noble-gas dependence of Rb line. They observed the spectra of blue satellite peak of Rb line in RbCl solutions dissolved with Ar or Kr. The position of the satellite peaks corresponded with those obtained in the gas-phase fluorescence experiments. They attributed the satellite peak to $B \rightarrow X$ transition of Rb–noble-gas van der Waals molecules. Choi et al. [50] also claimed the gas phase origin from the investigation of the effect of a small amount of ethanol on the Na line width and intensity. The line width increased with the ethanol concentration because of the collisional interactions of excited Na atoms with the hydrocarbon products of ethanol decomposition besides the interactions with noble gas. The observed quenching of Na emission upon addition of ethanol was accounted for by the interactions with unsaturated hydrocarbons and H_2, which are produced during the decomposition of ethanol.

The dissolved gas dependence of K emission was investigated in KCl solution by Hayashi and Choi[51] as shown in Fig. 11. The K line doublets at 766.6 and 770.0 nm for Xe (a) and Ar (b) saturation were asymmetrically broadened to the red side, while that for He (c) saturation was symmetrically broadened and slightly shifted to the blue side. The dashed lines in each figure indicate the normalized flame spectrum of KCl, which represents the instrumental spectral shape. These results agree well with the gas phase spectroscopic studies of alkali-metal atom emission52). Numerous data have been compiled on the line broadening and shift as functions of the density of foreign gas perturbers. The

result of the dissolved-gas effect suggests that the site of alkali-metal emission is the gas phase inside bubbles. Assuming an adiabatic compression process, they obtained the conditions of 3480 K and 585 atm at the bubble collapse. The only difference from the previous spectroscopic studies is the line shift for Xe and Ar perturbers. Although the line should be shifted to the red side according to the spectroscopic studies, the spectra in Figs. 11(a) and 11(b) seem to be unshifted from the original K doublet represented by the dashed line. This contradiction will be solved by considering two components of the K doublet, which are discussed later.

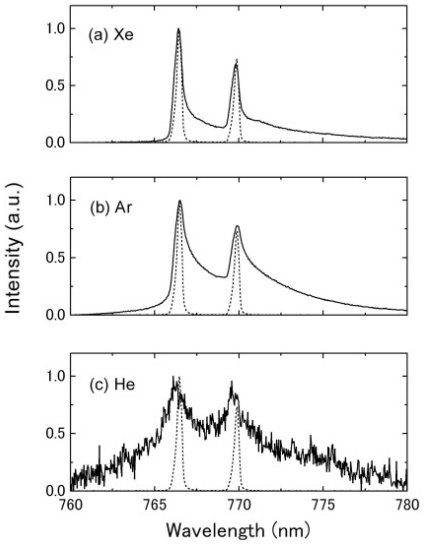

Fig. 11. Spectra of K atom emission from KCl solutions saturated with Xe (a), Ar (b) and He (c) at the temperature of 15 °C. The ultrasonic frequency and power used are 148 kHz and 2.3 W, respectively. A collecting time of the spectrometer was 1, 3 and 30 min. for the solutions saturated with Xe, Ar and He, respectively. All spectra are normalized at the maximum intensity. The dashed lines in each figure indicate the normalized flame spectrum of KCl. Reprinted with permission from ref. (50). Copyright 2012 by the American Chemical Society.

The effect of a surfactant, such as sodium dodecyl sulfate (SDS), on the behavior of a cavitation bubble extends in many ways, as reviewed by Ashokkumar and Grieser[53]. The effects on bubble dynamics such as rectified diffusion growth, bubble coalescence, and bubble size distribution cause the changes in SL intensity, final temperature at bubble collapse, and acoustic emission. It is interesting that Na emission is remarkably enhanced in SDS aqueous solution with the concentration of a few mM. SDS molecules adsorb at the bubble/liquid interface because of their hydrophobicity, inducing bubbles to be negatively charged. Na+ ions dissociated from SDS are attracted in the vicinity of the bubble/liquid interface by a Coulomb force. This situation is called the electric double layer. The local concentration of Na+ ions is, therefore, extremely high compared with the bulk of the solution. Sunartio et al.[54] reported that the intensity of Na emission in SDS solution was more than 100 times larger than that in NaCl solution. On the basis of this enhancement of Na emission in SDS solution, Sostaric et al.[55] proposed that the site of Na emission is a hot condensed phase at the bubble/liquid interface. They inferred that the electronical excitation of Na is made by the reduction of Na+ ions by water molecules in the ion's hydration shell.

Hayashi and Choi[56] carried out the spectroscopic study of the sonication-time effect on Na emission in SDS solution. Figure 12(a) shows an SL photograph from an argon-saturated 10 mM SDS solution contained in a cylindrical glass cell. The spatial distributions of Na emission (orange) and the continuum emission (blue white) are clearly separated, indicating that both emissions originate from different bubble populations. The SL spectra of Na emission were collected at every 3 min for the total

sonication time of 30 min. The spectra are shown in Fig. 12(b) for the cases of the sonication

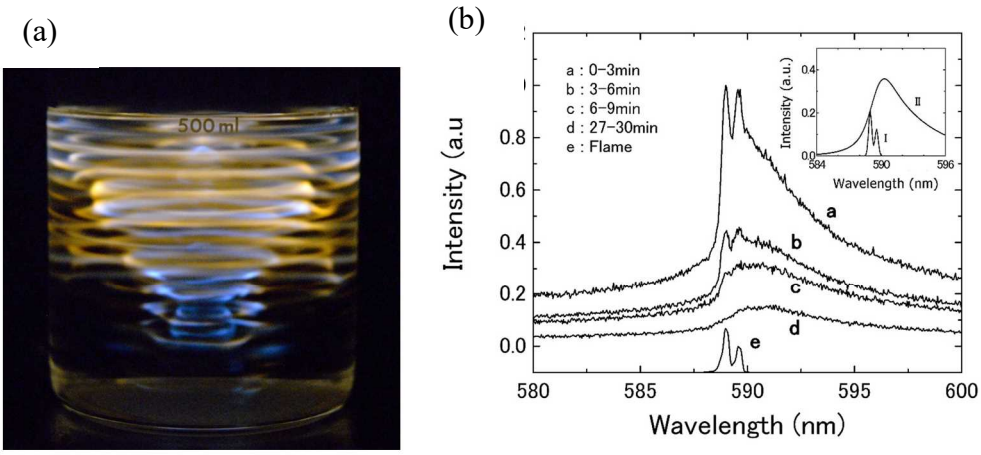

Fig.12. (Color online) (a): Photographic image of SL from Ar-saturated SDS aqueous solution at an acoustic power of 4.0 W. Ultrasound at a frequency of 148 kHz was irradiated from the bottom of the cylindrical container. An exposure time was 280 s. (b): SL spectra of Na emission from Ar-saturated SDS aqueous solutions at an acoustic power of 9.1 W. The spectra were collected every 3 minutes during a total sonication time of 30 minutes. The spectra are shown for the cases of 0-3, 3-6, 6-9 and 27-30 minutes, labeled a-d, respectively. The line labeled e denotes the spectrum obtained from NaCl in a flame. The inset shows the Na emission separated into two components for the case of 3-6 minutes: I, unshifted narrow lines; II, shifted broadened lines. Reprinted with permission from ref. (55). Copyright 2015 by Elsevier Publishing.

time of 0-3, 3-6, 6-9 and 27-30 min. labeled “a” to “d”, respectively. The line labeled “e” denotes the spectrum obtained from NaCl in a flame indicating the instrumental spectral shape. The intensity decreased with the sonication time, and interestingly spectral profile itself changed with the sonication time. This change in the spectral profile with the sonication time was not observed in NaCl solution. The intensity reduction in the Na spectrum can be explained by the decomposition of SDS molecules. The SDS molecules adsorbed on the bubble surface are injected into the bubble as droplets including the surrounding dense Na^+ ions, and are decomposed by heat and/or OH radical attack at bubble collapse, producing various decomposition gases such as H_2, CO and CH_4. These gases will quench the SL itself because the final temperature is reduced owing to the endothermic reactions of decomposition and a lower specific ratio of these gases compared with that of the noble gas. Further, these gases are known to have a direct quenching effect on Na emission. The variation of the spectral profile can be well understood if we consider that the Na lines are composed of two types of emission, narrow lines I and broadened lines II, as represented in the inset of Fig. 12(b). The narrow lines showed no line shift and their width was nearly equal to that of the flame spectrum e. The true width of the narrow line, therefore, cannot be known. The peaks of the broadened lines underwent a red shift from the original D lines and asymmetric broadening. The narrow lines were quenched at a higher rate than

the broadened lines with increasing sonication time. At the end of sonication, only the broadened lines remained. Using this two component model of the Na emission, the noble gas dependence of K spectrum shown in Fig. 11 can be elucidated. The broadened lines observed for the cases of Xe and Ar dissolution are interpreted as being red shifted.

A new question arises: what is the mechanism generating the narrow and broadened components? Is it possible to distinguish these two components experimentally? Nakajima et al. [57] performed experiments to separate the two components spatiotemporally by capturing the SL spatial distribution and SL pulses using different optical filters. A bandpass filter N centered at 589.3 nm with FWHM of 1.18 nm and a bandpass filter B centered at 592.5 nm with FWHM of 1.57 nm can transmit the narrow and broadened lines, respectively. The spectral profiles of Na emission using these filters are shown in Fig. 13(a). Figure 13(b) shows SL image from 4 M NaCl solution saturated with Kr at 145 kHz using no filter. Figures 13 (c) and (d) show the SL images from the NaCl solution using filter N and B, respectively. The emission of the narrow component, as shown in Fig. 13(c), is relatively strong in the region near the center of the cylindrical cell where the sound pressure is relatively high. The emission of the broadened component, as shown in Fig. 13(d), extends in the region near the side wall of the cell and liquid surface where the sound pressure is relatively low. The difference in the spatial distribution suggests that the two components originate from different bubble populations and also that the narrow component arises from bubbles with a collapse temperature higher than that in the case of the broadened component. If the narrow component originated from the bubble/liquid interface where the temperature may be lower than that inside the bubble, the narrow component would always be present whenever conditions are sufficient to give rise to the broadened component inside the bubble [58]. The different bubble populations of the two components were ascertained in the experiment of SL pulses. When the SL pulses of the narrow component were observed, no pulses of the broadened component were observed simultaneously.

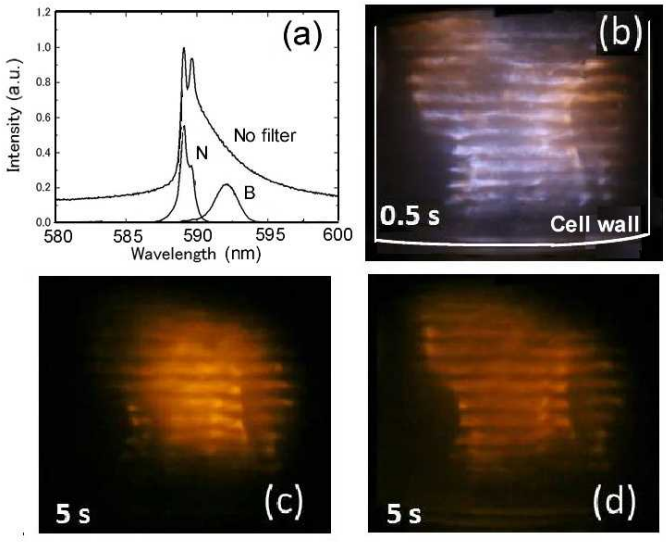

Fig. 13. (Color online) Spatial separation of the narrow and broadened lines of Na emission. (a): Spectral profiles of Na emission obtained using no filter, and using filter N and B. (b): SL image from from 4 M NaCl solution captured with a Canon EOS 6D camera using no filter. (c):SL image from 4 M NaCl solution captured with using filter N. (d): SL image from 4 M NaCl solution captured with using filter B. Exposure time is indicated in the bottom of the images. Reprinted with permission from ref. (56). Copyright 2015 by the Japan Society of Applied Physics.

The results by the present author's group on alkali-metal emission showed that alkali-metal atom emission includes the broadened and narrow components, and the blue satellite peak. The broadened component and the blue satellite peak originate from strong interactions between alkali-metal atoms and a noble gas in the bubble. Figure 14 illustrates a schematic image of the potential energy and electronic transitions of a van der Walls molecule consisting of a Na atom and a noble gas atom. The potential energy curves representing the states of $X^2\Sigma+$ (the ground state), $A^2\Pi$ (the first excited state), and $B^2\Sigma+$ (the second excited state) are plotted as a function of Na–noble gas atom distance59). Original Na D lines are represented by the transition of 3P–3S in which the interatomic distance is sufficiently large. The broadened component is attributable to the transition of $A^2\Pi$–$X^2\Sigma+$ (red arrow), and the blue satellite peak corresponds to the transition of $B^2\Sigma+$–$X^2\Sigma+$ (blue arrow)49). The origin of the narrow component is uncertain at the present stage. Compared with the broadened component, the narrow component is easily subjected to the effects of a foreign gas. The narrow component was not observed in the solution dissolved with He or Ne, and was enhanced in the solution dissolved with Ar, Kr, or Xe. The narrow component is dominant under sonication at a frequency of 1 MHz. SBSL spectrum of Na emission included only narrow component60). These findings suggest that the narrow component may originate from bubbles of higher temperature than those for the broadened component. Further research is needed to clarify the exact mechanism of the narrow component.

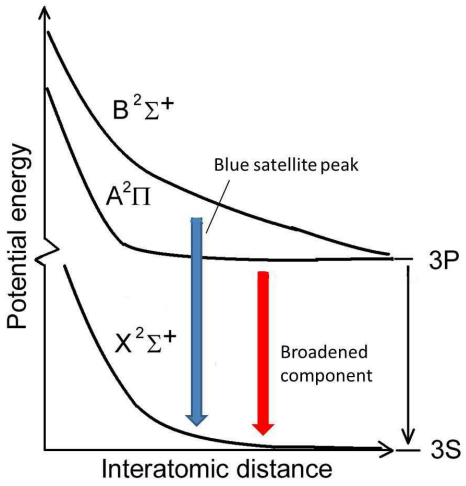

Fig. 14. (Color online) Potential energy curves vs. interatomic distance between Na and a noble gas atom. The transition 3P-3S indicates the original D lines.

4.4 Sonoluminescence using a horn-type transducer

A horn-type transducer is frequently used in various applications in industrial engineering and sonochemistry. The most different feature from a plate-type transducer is the acoustic power density. A power on the order of hundreds of W/cm2 can be achieved with the horn-type transducer, whereas a power of a few W/cm^2 is typical for the plate-type transducer. The frequency of the horn-type transducer is confined to around 20 kHz. Vast numbers of bubbles are produced owing to strong acoustic pressure radiated by the horn-type transducer. The spatial distribution of SL exhibits a distinct wedge shape under the horn surface in water. Figure 15 shows some examples of photographic images of SL at 24 kHz observed in water, 1 M NaCl solution and 68% glycerin aqueous solution. The radiated

powers are 4.2, 17, and 67 W/cm^2 from the upper to the lower row[61]. In the cases of water and NaCl

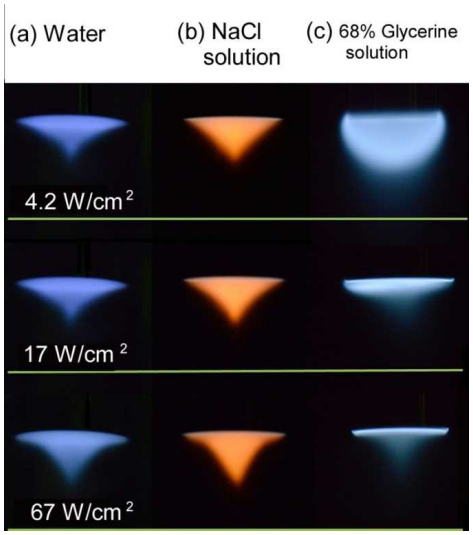

Fig.15. (Color online) Sonoluminescence from water, 1 M NaCl solution and 68% glycerin solution using a horn-type transducer at a frequency of 24 kHz and powers of 4.2, 17 and 67 W/cm^2 from top to bottom.

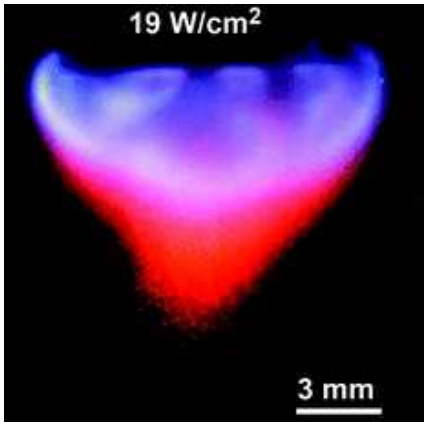

Fig.16. Sonoluminescence from 0.1 M Na_2SO_4 in 95% sulfuric acid using a horn transducer, demonstrating the separation of orange Na emission from blue-white continuum emission. Reprinted with permission from ref. (61). Copyright 2009 by American Chemical Society.

solution, the spatial distributions show the wedge shape at all powers. In the case of 68% glycerin aqueous solution, the spatial distribution shows a bulbous shape only at 4.2 W/cm^2. This contrast is caused by the difference in bubble structure generated in the solution with a different viscosity. The cause of the conical bubble structure was explained by Dubas et al.[62] The bubble layer is formed on the horn surface with a higher bubble density at the center and a lower bubble density at the periphery, acting like a sound-field focusing lens. The amplitude of sound field attenuates rapidly by the high-density bubbles. This causes the conical bubble structure, resulting in the wedge shape of SL distribution. The bulbous shape in 68% glycerin solution at 4.2 W/cm^2 may be caused by the absence of the bubble layer on the horn surface and hence the absence of the lensing effect. The absence of the bubble layer is attributed to the change in bubble dynamics caused by the high viscosity. The bubbles in viscous liquid are smaller and more spherical than those in water. An exact explanation of this bubble dynamics needs further research. Using a horn transducer, Xu et al. [62] reported clear separation of orange Na emission from blue-white continuum emission in a solution of 0.1 M Na_2SO_4 in 95% sulfuric acid, as shown in Fig. 16. Na emission arises from rapidly moving bubbles in a streaming liquid flow outside of the dense clouds, whose collapse is much less symmetric and from which emission from nonvolatiles becomes possible through the mechanism of nanodroplet injection [63]. This observation favors the droplet model over the heated shell model of Na emission.

5. Summary and conclusions

Acoustic cavitation provides a unique field of high-temperature and high-pressure conditions

that are created by the implosive bubble collapse. Chemical reactions and light emission are generated under these extreme conditions. The fundamentals of bubble dynamics and mechanism of SL were briefly reviewed together with some experimental results. The bubble–bubble interactions cause bubble oscillation to be nonspherical and also cause bubbles to form a cluster or cloud. Hence the bubble dynamics have a strong effect on SL intensity.

SL from alkali-metal salt solution has long been interested. Our experimental results of spectroscopic studies on alkali-metal atom emission strongly suggested that the location of the emission site is in the gas phase inside bubbles. The bubble population generating the alkali-metal atom emission and blue white continuum emission is quite different in MBSL. The alkali-metal atom emission arises from lower temperature bubble which oscillates nonspherically. The emission line is broadened and shifted from the original D line, and this is because van der Waals molecules are formed between the alkali-metal atom and noble-gas atom. The alkali-metal atom line which exhibits no broadening and no shift was newly found to superpose on the broadened and shifted line. The new line may originate from a higher temperature condition in the bubble, but the exact origin is unresolved. Nonvolatile alkali-metal ions enter bubble by means of liquid droplets at the events of bubble coalescence and fragment. This conclusion may provide useful information on the application of sonochemistry in solutions including nonvolatile species.

Acknowledgments

The author thanks all of the past and present members of Physical Ultrasonics group of Meiji University, in particular Yuichi Hayashi.

References

1) F. R. Young, Sonoluminescence (CRC press, Boca Raton, FL, 2005).
2) P. Brenner, S. Hilgenfeldt, and D. Lohse, Rev. Mod. Phys. 74, 425 (2002).
3) B. P. Barber, R. A. Hiller, R. Lofstedt, S. Putterman and K. R. Weninger, Phys. Rep. 281, 65 (1997).
4) K. Yasui, T. Tuziuti, M. Sivakumar, and Y. Iida, Appl. Spectrosc. Rev. 39, 399 (2004).
5) H. Frenkel and H. Schultes, Z. Phys. Chem. 27, 421 (1934).
6) E. N. Harvey, J. Am. Chem. Soc. 61, 2392 (1939).
7) T. G. Lighton, The Acoustic Bubble (Academic Press, London, 1994).
8) F. R. Young, Cavitation (Imperial College Press, London, 1999).
9) W. Lauterborn and T. Kurz, Rep. Prog. Phys. 73, 106501 (2010).
10) R. W. Wood and A. L. Loomis, Philos. Mag. 4, 417 (1927).
11) Sonochemistry and the Acoustic Bubble, ed. F. Grieser, P.-K. Choi, N. Enomoto, H. Harada, K. Okitsu, and K. Yaui, (Elsevier, Amsterdam, 2014).
12) Handbook of Ultrasonics and Sonochemistry, ed. M. Ashokkumar (Springer, Singapore, 2016).
13) R. Reisz and T. Kondo, Free Radicals Biol. Med. 13, 247 (1992).
14) Y. Yoshimura, M. So, H. Yagi, and Y. Goto, Jpn. J. Appl. Phys. 52, 07HA01 (2013).

15) H. Hamada, H. Ogi, K. Noi, H. Yagi, Y. Goto, and M. Hirao, Jpn. J. Appl. Phys. 54, 07HE01 (2015).
16) M. Matsuoka, F. Takahashi, Y. Asakura, and J. Jin, Jpn. J. Appl. Phys. 55, 07KB01 (2016).
17) S. Umemura, S. Yoshizawa, R. Takagi, Y. Inaba, and J. Yasuda, Jpn. J. Appl. Phys. 52, 07HA02 (2013).
18) J. Yasuda, T. Miyashita, K. Taguchi, S. Yoshizawa, and S. Umemura, Jpn. J. Appl. Phys. 54, 07HF21 (2015).
19) J. Yasuda, S. Yoshizawa, and S. Umemura, Jpn. J. Appl. Phys. 55, 07KF24 (2016).
20) C. Honma, D. Kobayashi, H. Matsumoto, T. Takahashi, C. Kuroda, K. Otake, and A. Shono, Jpn. J. Appl. Phys. 52, 07HE11 (2013).
21) Y. U. Kim, S. H. Park, J. H. Moon, and S. M. Jang, Jpn. J. Appl. Phys. 52, 07HE09 (2013).
22) E. Cho, J. Choi, Y. Lee, J. Min Park, and J. Khim, Jpn. J. Appl. Phys. 52, 07HE08 (2013).
23) T. Takahashi, N. Takada, and H. Toyoda, Jpn. J. Appl. Phys. 53, 07KE01 (2014).
24) M. Lim, S. Na, J. Khim, and Y. Son, Jpn. J. Appl. Phys. 53, 07KE02 (2014).
25) D. Kobayashi, C. Honma, H. Matsumoto, T. Takahashi, Y. Shimada, C. Kuroda, K. Otake, and A. Shono, Jpn. J. Appl. Phys. 53, 07KE03 (2014).
26) K. Shimakage, D. Kobayashi, M. Naya, H. Matsumoto, Y. Shimada, K. Otake, and A. Shono, Jpn. J. Appl. Phys. 55, 07KE01 (2016).
27) S. Nomura, S. Miyagawa, S. Mukasa, and H. Toyota, Jpn. J. Appl. Phys. 55, 07KE02 (2016).
28) J. Kim, J. Kim, K. Ha, and M. Kim, Jpn. J. Appl. Phys. 55, 07KE03 (2016).
29) S. Kim, W. Lee, and Y. Son, Jpn. J. Appl. Phys. 55, 07KE04 (2016).
30) R. K. Bhaskaracharya, S. Kentish, and M. Ashokkumar, Food Eng. Rev. 1, 31 (2009).
31) J. B. Keller, and M. Miksis, J. Acoust. Soc. Am. 68, 628 (1980).
32) T. Kozuka, S. Hatanaka, K. Yasui, T. Tujiuti, and H. Mitome, Jpn. J. Appl. Phys. 41, 3248 (2002).
33) Y. Hayashi and P.-K. Choi, Ultrasonics 44, e421 (2006).
34) H. Mitome, Jpn. J. Appl. Phys. 40, 3484 (2001).
35) A. Henglein and M. Gutierrez, J. Phys. Chem. 94, 5169 (1990).
36) S. Hatanaka, K. Yasui, T. Kozuka, T. Tuziuti, and H. Mitome, Ultrasonics 40, 655 (2002).
37) K. V. B. Tran, Y. Asakura, and S. Koda, Jpn. J. Appl. Phys. 52, 07HE07 (2013).
38) Y. Uemura, K. Sasaki, K. Minami, T. Sato, P.-K. Choi, and S. Takeuchi, Jpn. J. Appl. Phys. 54, 07HB05 (2015).
39) H.-B. Lee and P.-K. Choi, Ultrason. Sonochem. 21, 2037 (2014).
40) K. S. Suslick and D. J. Flannigan, Annu. Rev. Phys. Chem. 59, 659 (2008).
41) K. S. Suslick, N. C. Eddingsaas, D. J. Flannigan, S. D. Hopkins, and H. Xu, Ultrason. Sonochem. 18, 842 (2011).
42) J. B. Young, J. A. Nelson, and W. Kang, Phys. Rev. Lett. 86, 2673 (2001).
43) H. Xu and K. S. Suslick, Phys. Rev. Lett. 104, 244301 (2010).
44) S. Abe and P.-K. Choi, Jpn. J. Appl. Phys. 48, 07GH02 (2009).
45) P.-K. Choi, in Theoretical and Experimental Sonochemistry Involving Inorganic Systems, ed. Pankaj and M. Ashokkumar (Springer, Heiderberg, 2010) p. 337.

46) P. Günther, W. Zeil, U. Grisar, and E. Heim, Z. Electrochem. 61, 188 (1957) [in German].
47) C. Sehgal, R. P. Steer, R. G. Sutherland, and R. E. Verrall, J. Chem. Phys. 70, 2242 (1979).
48) E. B. Flint and K. S. Suslick, J. Phys. Chem. 95, 1484 (1991).
49) F. Lepoint-Mullie, N. Voglet, T. Lepoint, and R. Avni, Ultrason. Sonochem. 8, 151 (2001).
50) P.-K. Choi, S. Abe, and Y. Hayashi, J. Phys. Chem. B 112, 918 (2008).
51) Y. Hayashi and P.-K. Choi, J. Phys. Chem. B 116, 7891 (2012).
52) N. Allard and J. Kielkopf, Rev. Mod. Phys. 54, 1103 (1982).
53) M. Ashokkumar and F. Grieser, Phys. Chem. Chem. Phys. 9, 5631 (2007).
54) D. Sunartio, K. Yasui, T. Tuziuti, T. Kozuka, Y. Iida, M. Ashokkumar, and F. Grieser, ChemPhysChem, 8, 2331 (2007).
55) J. Z. Sostaric, M. Ashokkumar, and F. Grieser, Langmuir, 32, 12387 (2016).
56) Y. Hayashi and P.- K. Choi, Ultrason. Sonochem. 23, 333 (2015).
57) K. Nakajima, Y. Hayashi, and P.-K. Choi, Jpn. J. Appl. Phys. 54, 07HE02 (2015).
58) H. Xu, N. C. Eddingsaas, and K. S. Suslick, J. Am. Chem. Soc. 131, 6060 (2009).
59) B. C. Laskowski, S. R. Langhoff, and J. R. Stallcop, J. Chem. Phys. 75, 815 (1981).
60) P.-K. Choi, K. Takumori, and H.-B. Lee, Ultrason. Sonochem. 38, 154 (2017).
61) T. Yamada and P.-K. Choi, Proc. 32nd Symp. Ultrasonic Electronics, 2011, p. 385.
62) B. Dubus, C. Vanhille, C. Campos-Pozuelo, and C. Granger, Ultrason. Sonochem. 17, 818 (2010).
63) H. Xu, N. C. Eddingsaas, and K. S. Suslick, J. Am. Chem. Soc. 131, 6060 (2009).
64) S. Hatanaka, S. Hayashi, and P.-K. Choi, Jpn. J. Appl. Phys. 49, 1347 (2010).